Electronic Supplementary Material (ESI) for Journal of Materials Chemistry A.

Supporting Information for

A hybrid coupling of MIL-53(Fe) and conductive sulfide as a synergistic electrocatalyst for oxygen evolution reaction

Fang Wu,[a] Xiaoxue Guo,[a] Qinghua Wang,[c] Suwei Lu,[b] Jinling Wang,[a] Yubing Hu,[a] Gazi Hao,[a] Qiulin Li,[a] Min-Quan Yang,*[b] Wei Jiang*[a]

E-mail: superfine_jw@126.com; yangmq@fjnu.edu.cn

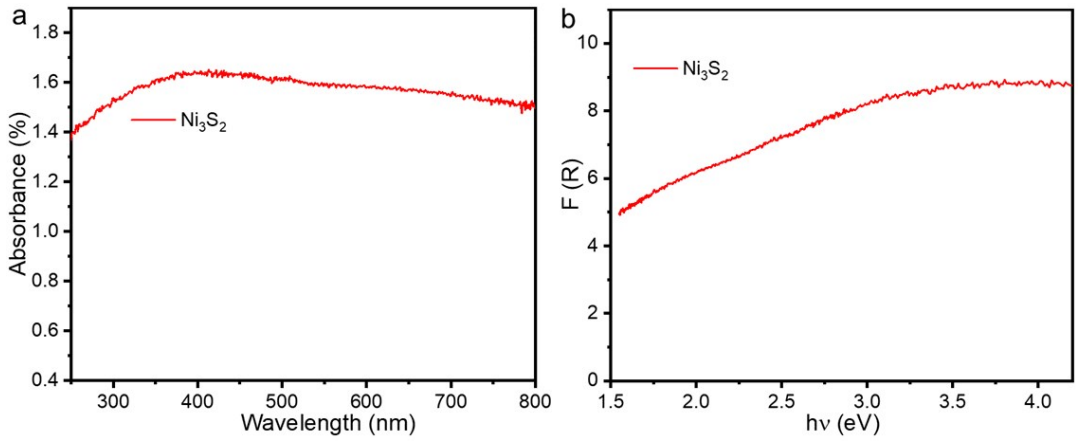

Fig. S1 UV−visible diffuse reflectance spectra (DRS) of the Ni_3S_2 sample (a); and the plot of transformed Kubelka−Munk function versus the energy of light (b).

Note: Fig. S1 shows the UV-visible diffuse reflectance spectroscopy (DRS) of Ni_3S_2, which is an effective technique for analyzing the bandgap of the material. The result reveals that the Ni_3S_2 has a broadband light absorption in the UV-visible range, without absorption edge. Correspondingly, the band gap of the Ni_3S_2 is calculated from the plot of the transformed Kubelka−Munk function versus the energy of light. No obvious bandgap is observed. The result is well consistent with the theoretical calculation, demonstrating the metallic characteristic of the Ni_3S_2.[S1-S3]

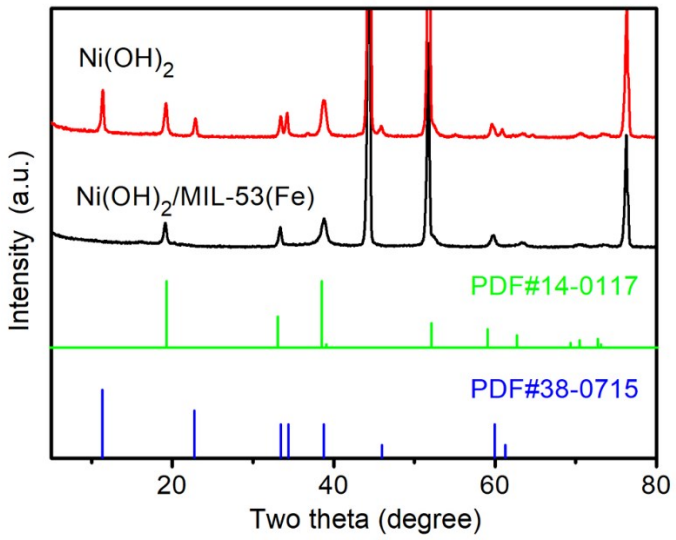

Fig. S2 XRD patterns of $Ni(OH)_2$, $Ni(OH)_2$/MIL-53(Fe).

Note: As can be seen from **Fig. S2**, the diffraction peaks of the bare $Ni(OH)_2$ are matched with the standard α-$Ni(OH)_2$ (JCPDS No. 38-0715) and β-$Ni(OH)_2$ (JCPDS No. 14-0117). In comparison, the XRD spectrum of the $Ni(OH)_2$/MIL-53(Fe) only shows the characteristic peaks of β-$Ni(OH)_2$. The disappearance of α-$Ni(OH)_2$ diffraction peaks can be ascribed to the phase transformation of α-$Ni(OH)_2$ to β-$Ni(OH)_2$ in DMF solution. This is because DMF is a basic solvent.[S4,S5] Especially, it will decompose to generate amine under hydrothermal condition,[S6] which can further enhance the alkalinity of the solution. Meanwhile, α-$Ni(OH)_2$ is very unstable in alkali and can quickly transform into the β-phase.[S7] Therefore, for the synthesis of $Ni(OH)_2$/MIL-53(Fe), after the hydrothermal treatment in DMF solution, only β-$Ni(OH)_2$ is obtained.

Notably, despite that the phase of nickel hydroxide in bare $Ni(OH)_2$ and $Ni(OH)_2$/MIL-53(Fe) is different, it has no critical influence on the activity improvement between final products of Ni_3S_2 and Ni_3S_2/MIL-53(Fe). Because after sulfurization, the phase of nickel sulfide in bare Ni_3S_2 and hybrid Ni_3S_2/MIL-53(Fe) is the same.

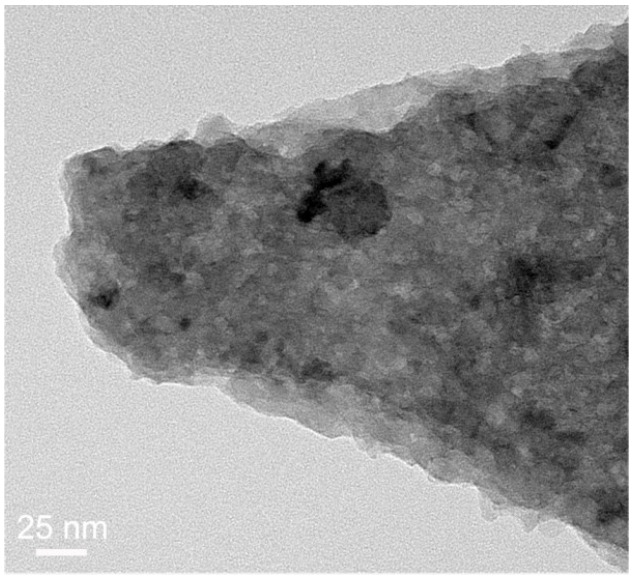

Fig. S3 TEM image of Ni_3S_2.

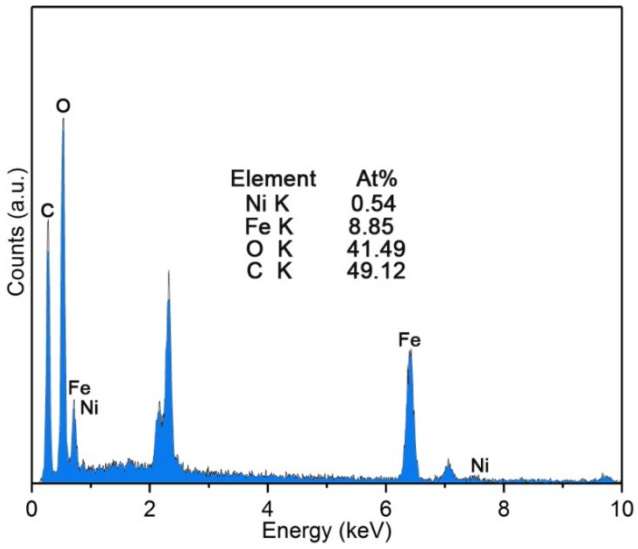

Fig. S4 SEM-EDX spectrum of MIL-53(Fe) powder collected from the bottom of autoclave.

Note: To verify that the released Ni^{2+} is included into the formation of MOFs during the synthesis of Ni_3S_2/MIL-53(Fe), SEM-EDX and ICP measurements of MIL-53(Fe) powder collected from the bottom of autoclave are performed. As shown in **Fig. S4**, The SEM-EDX spectrum shows an obvious Ni peak of the MIL-53(Fe) powder. The Ni/Fe atomic ratio is calculated to be 1:16.4. ICP analysis of the as-synthesized MIL-53(Fe) powder also verifies the presence of Ni, with a Ni/Fe molar ratio of about 1:16. Since that no extra Ni source is introduced during the hydrothermal process, the result confirms that the released Ni^{2+} is included into the formation of the MOF.

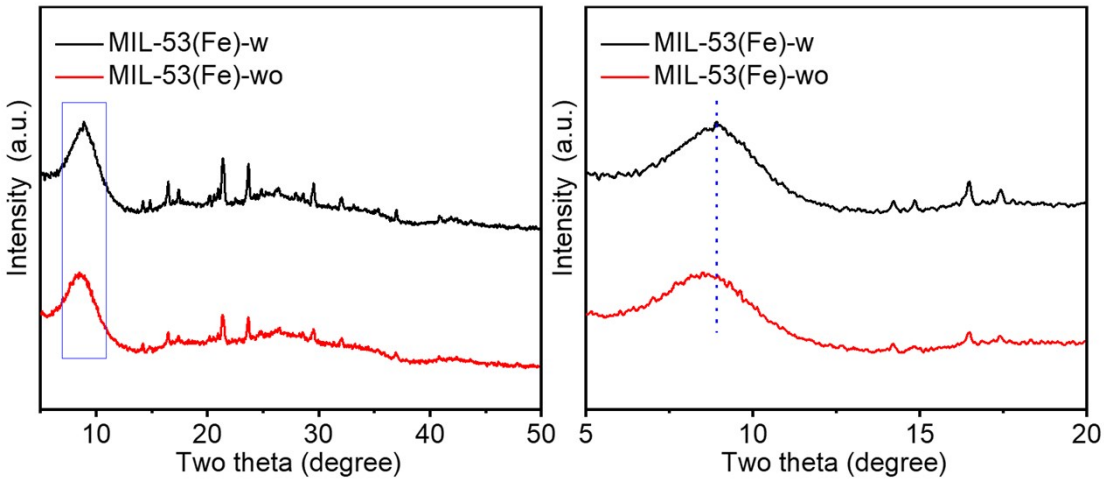

Fig. S5 XRD patterns of MIL-53(Fe) powder obtain with the synthesis of hybrid Ni_3S_2/MIL-53(Fe) (-w) and MIL-53(Fe) alone (-wo).

Note: To verify that the released Ni^{2+} is able to coordinate with the organic ligand instead of being adsorbed into MIL-53, XRD analyses of the MIL-53(Fe)-w powder (obtained with the presence of Ni_3S_2) and its counterpart of MIL-53(Fe)-wo (obtained without the presence of Ni_3S_2) collected from the bottom of autoclave are performed. As shown in **Fig. S5**, the XRD pattern of the MIL-53(Fe)-w shows similar diffraction peaks as that of MIL-53(Fe)-wo, except that the characteristic peak of MIL-53(Fe) at ~8.8° shifts to high 2θ value. This shift can be ascribed to the incorporation of Ni ions into the MIL-53(Fe), which has been commonly observed in bimetal MOFs.[S8,S9] Therefore, in combine the XRD analysis with the SEM-EDX and ICP characterizations, it can be concluded that Ni^{2+} is included into the formation of MIL-53(Fe) MOF.

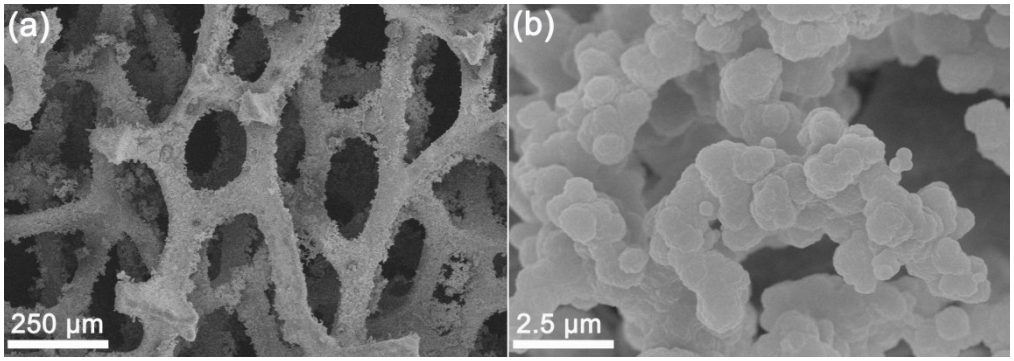

Fig. S6 SEM images of MIL-53(Fe).

Note: Fig. S6 shows the SEM images of the MIL-53(Fe)/NF. It reveals that the surface of the NF is covered by plenty of large MIL-53(Fe) particles after the hydrothermal process, which are severely agglomerated.

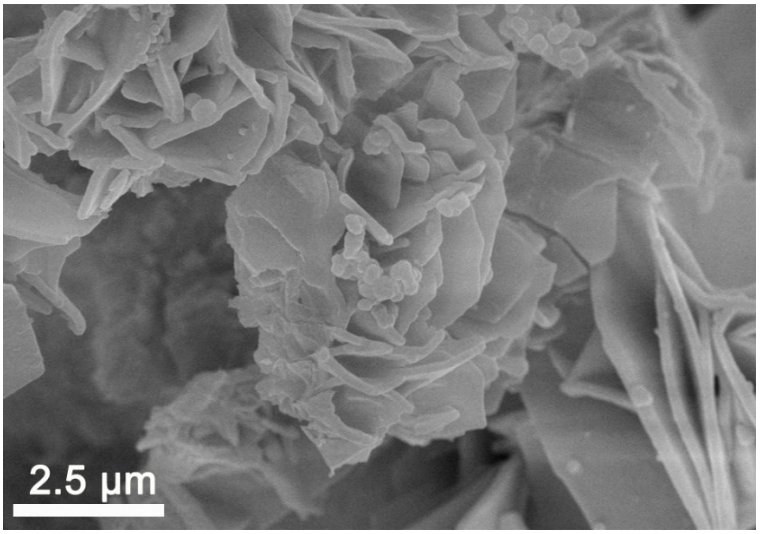

Fig. S7 SEM image of $Ni(OH)_2$/MIL-53(Fe).

Note: Fig. S7 shows the SEM images of the $Ni(OH)_2$/MIL-53(Fe). It suggests that the surface of the $Ni(OH)_2$ is covered by a layer of MIL-53(Fe) after the hydrothermal process.

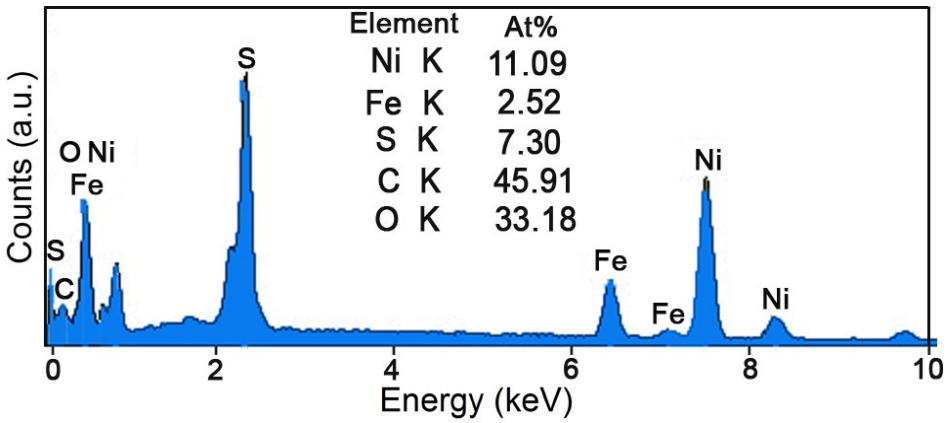

Fig. S8 SEM-EDX spectrum of Ni_3S_2/MIL-53(Fe).

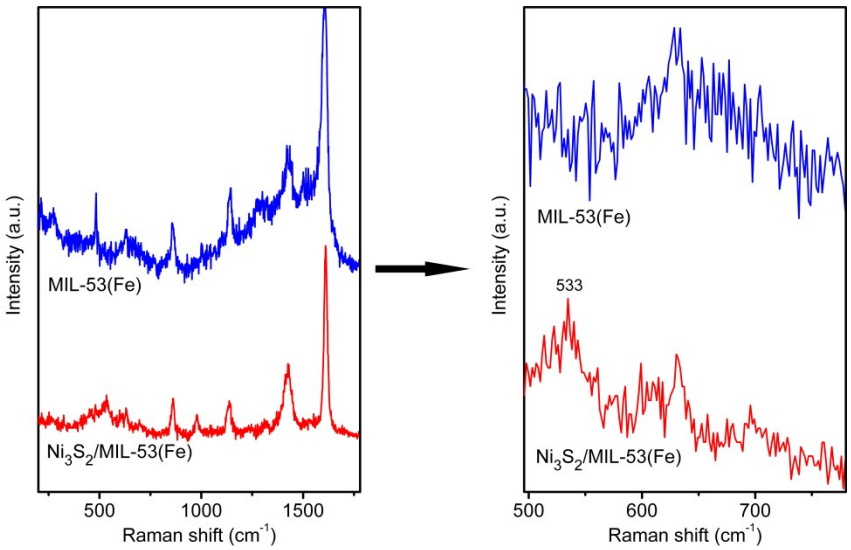

Fig. S9 Raman spectra of MIL-53(Fe) and Ni_3S_2/MIL-53(Fe).

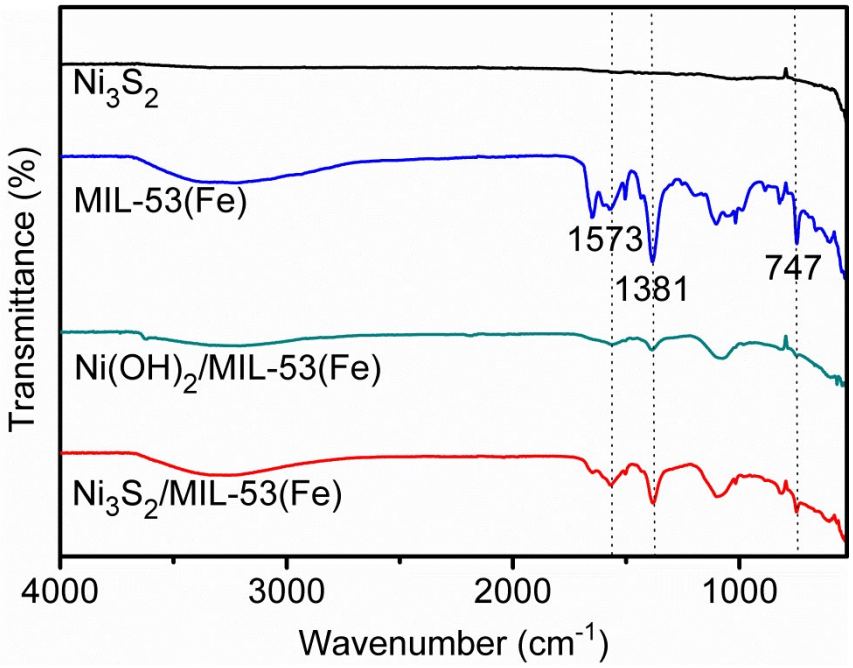

Fig. S10 FT-IR spectra of Ni_3S_2, MIL-53(Fe), $Ni(OH)_2$/MIL-53(Fe) and Ni_3S_2/MIL-53(Fe).

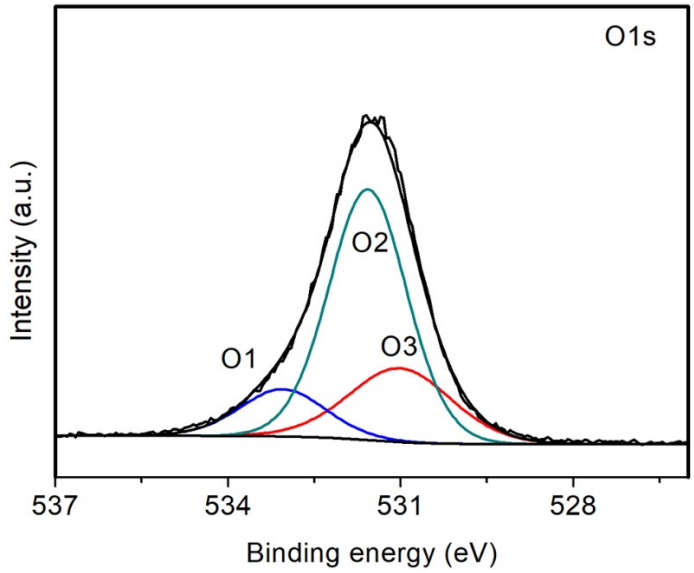

Fig. S11 High-resolution O 1s XPS spectrum of Ni_3S_2/MIL-53(Fe).

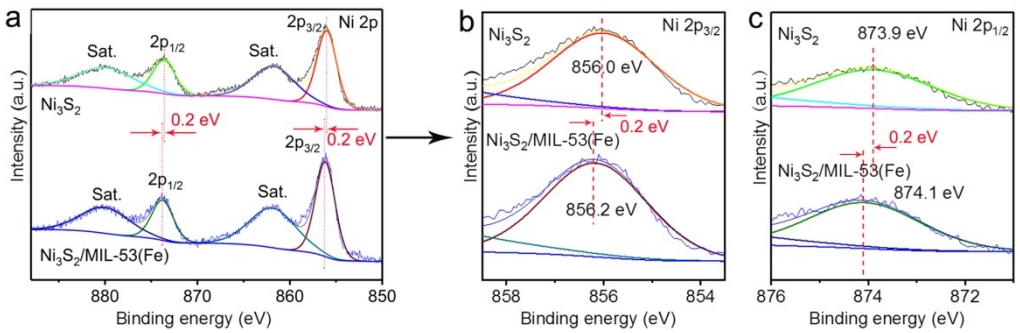

Fig. S12 XPS spectra of Ni 2p for Ni_3S_2 and Ni_3S_2/MIL-53(Fe).

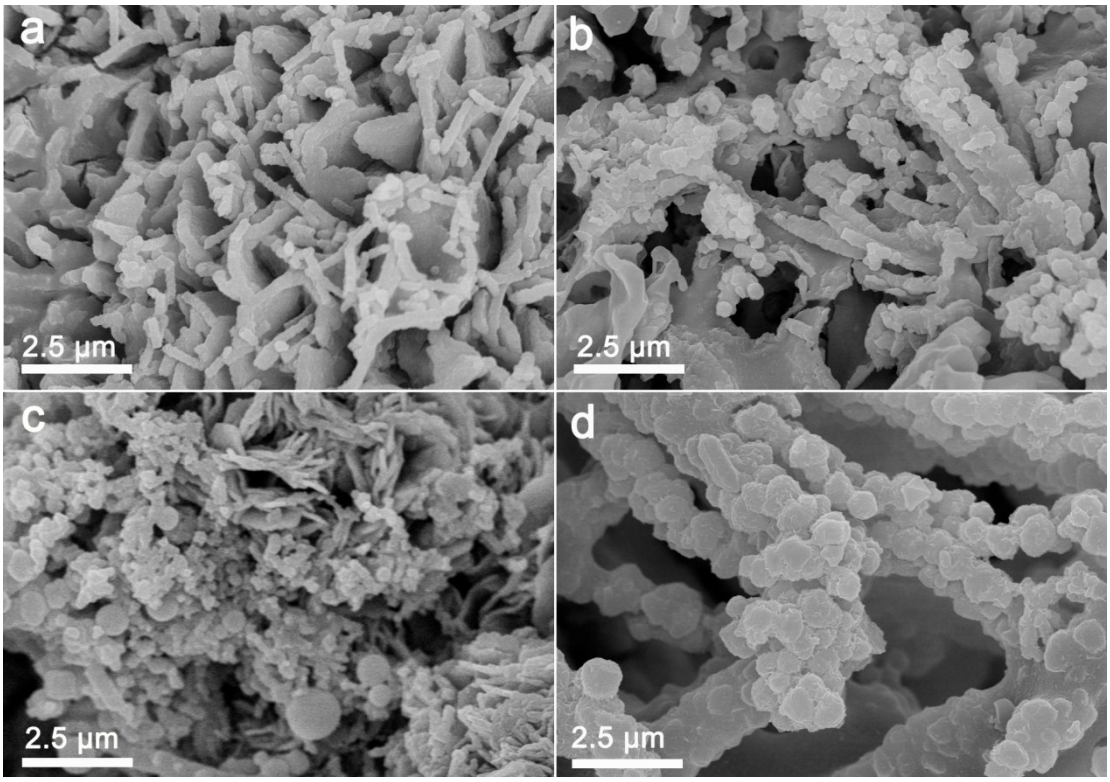

Fig. S13 SEM images of Ni_3S_2/MIL-53(Fe) with different hydrothermal time: (a) 1.5 h, (b) 6 h, (c) 9 h, (d) 12 h.

Note: The SEM images of the series of Ni_3S_2/MIL-53(Fe) samples reveal that with the increase of hydrothermal time, bigger and agglomerated MIL-53(Fe) nanoparticles are observed. This can be explained as the continued growth of MOFs.

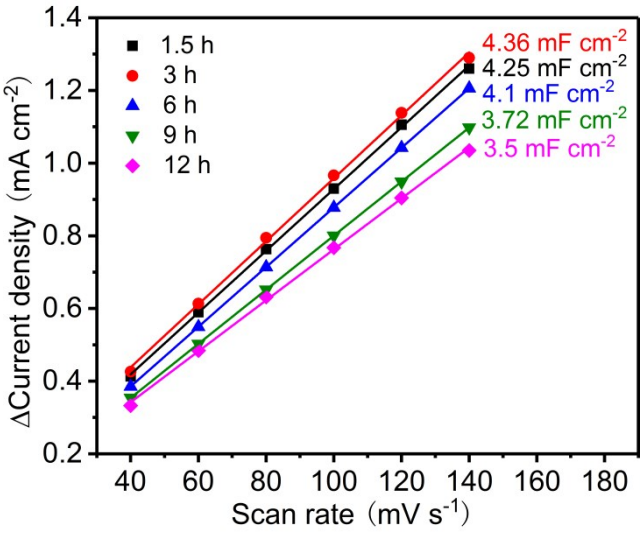

Fig. S14 The plots of ΔJ versus scan rates for Ni_3S_2/MIL-53(Fe) with different hydrothermal time.

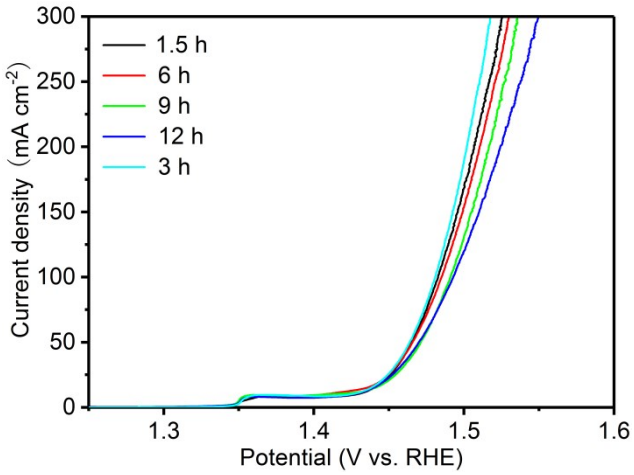

Fig. S15 Polarization curves of Ni_3S_2/MIL-53(Fe) with different hydrothermal time.

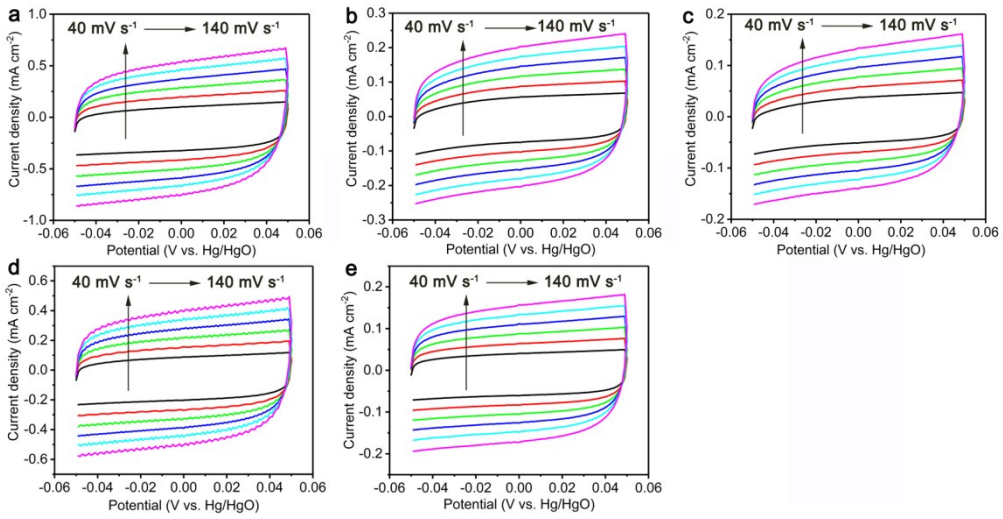

Fig. S16 CV curves of (a) Ni_3S_2/MIL-53(Fe), (b) MIL-53(Fe), (c) $Ni(OH)_2$/MIL-53(Fe), (d) Ni_3S_2, and (e) $Ni(OH)_2$ at different scan rates in the potential range of -0.05−0.05 V vs. Hg/HgO region.

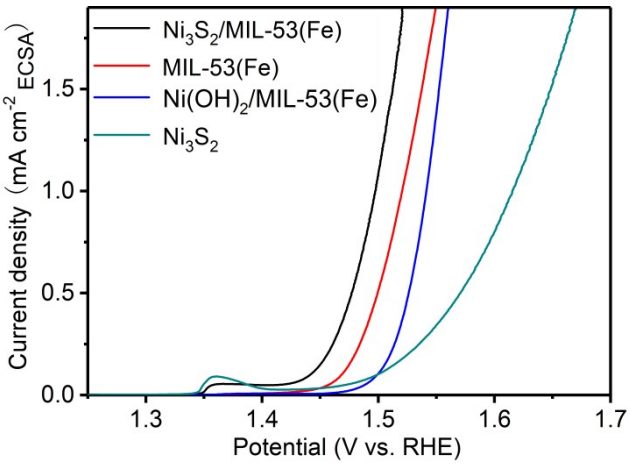

Fig. S17 ECSA-normalized polarization curves for Ni_3S_2/MIL-53(Fe), MIL-53(Fe), $Ni(OH)_2$/MIL-53(Fe) and Ni_3S_2.

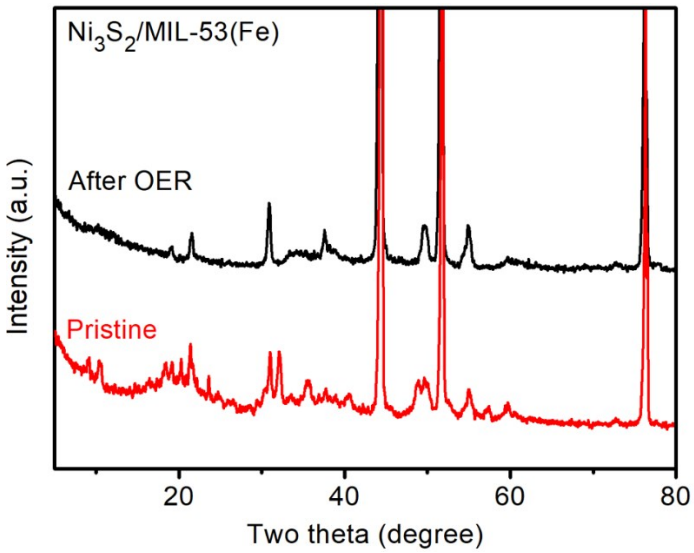

Fig. S18 XRD patterns of Ni_3S_2/MIL-53(Fe) before and after OER stability test.

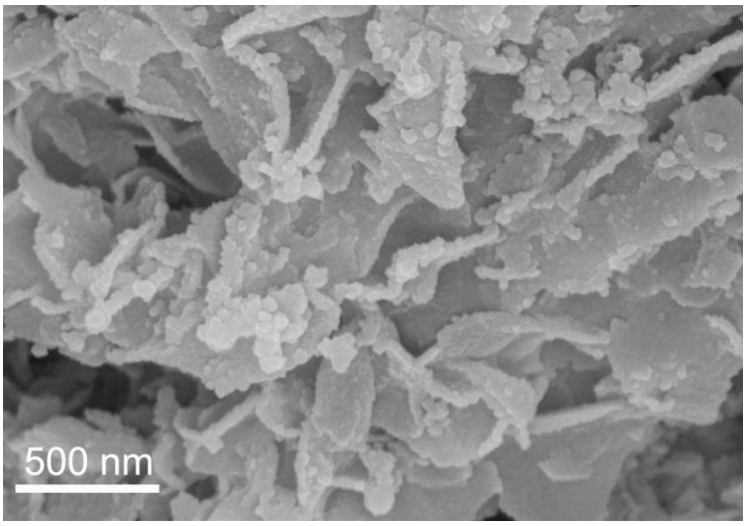

Fig. S19 SEM image of Ni_3S_2/MIL-53(Fe) after OER stability test.

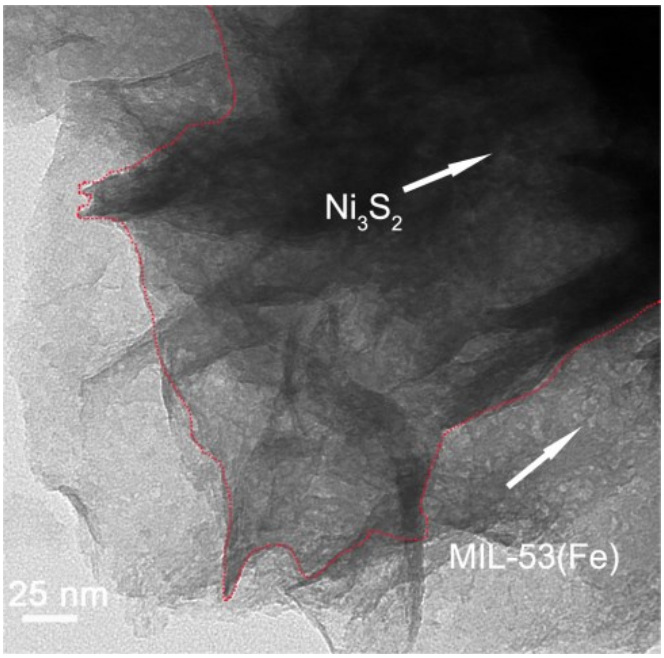

Fig. S20 TEM image of Ni_3S_2/MIL-53(Fe) after OER stability test.

Note: After stability test, as shown in **Fig. S20**, it can be seen that the strong color contrast between the inner component and the outer layer is similar to that of the fresh sample, which indicates that the structure of the Ni_3S_2/MIL-53(Fe) in micrometer size is maintained. That is, the Ni_3S_2 is covered by the MIL-53(Fe) layer. Moreover, due to the decomposition of organic ligand of the MOFs during electrocatalytic activity test, many pores will be generated in the MOF structure. This has been demonstrated in MOFs electrocatalysts.[S10] Therefore, it can be deduced that in the TEM image of the used Ni_3S_2/MIL-53(Fe), the deep colored part is Ni_3S_2, while the light colored part with pores is MIL-53(Fe) layer.

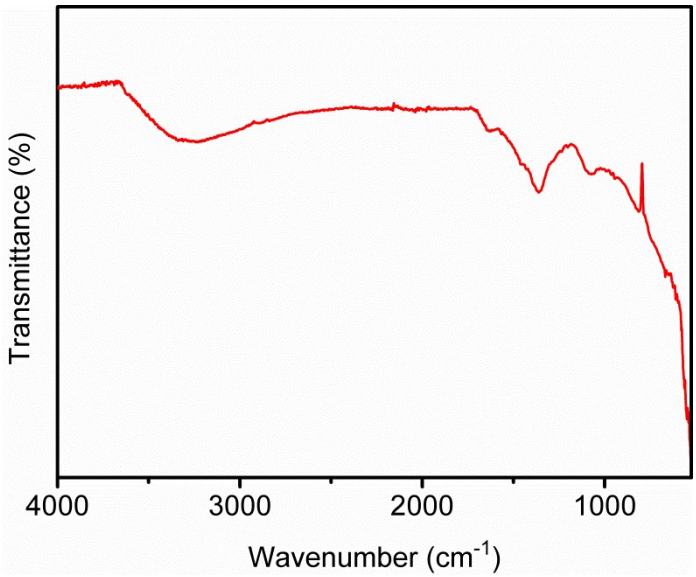

Fig. S21 FT-IR spectrum of Ni_3S_2/MIL-53(Fe) after OER stability test.

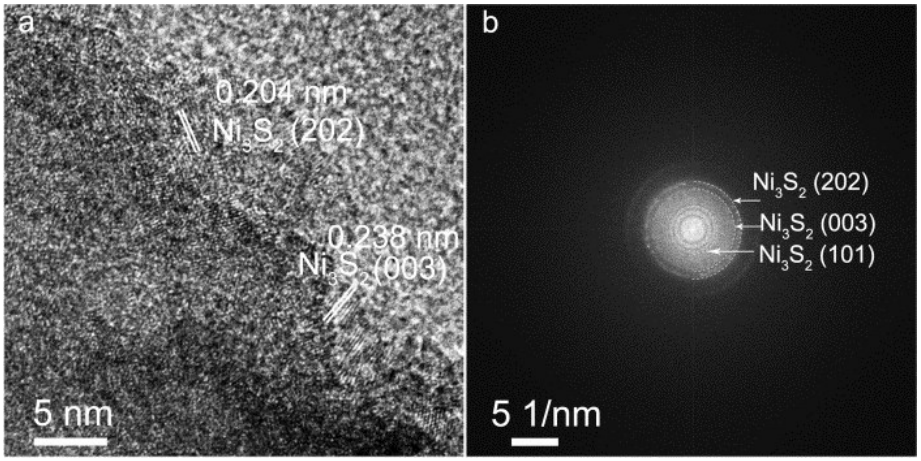

Fig. S22 (a) HRTEM image, and (b) the corresponding SAED pattern of Ni_3S_2/MIL-53(Fe) after OER stability test.

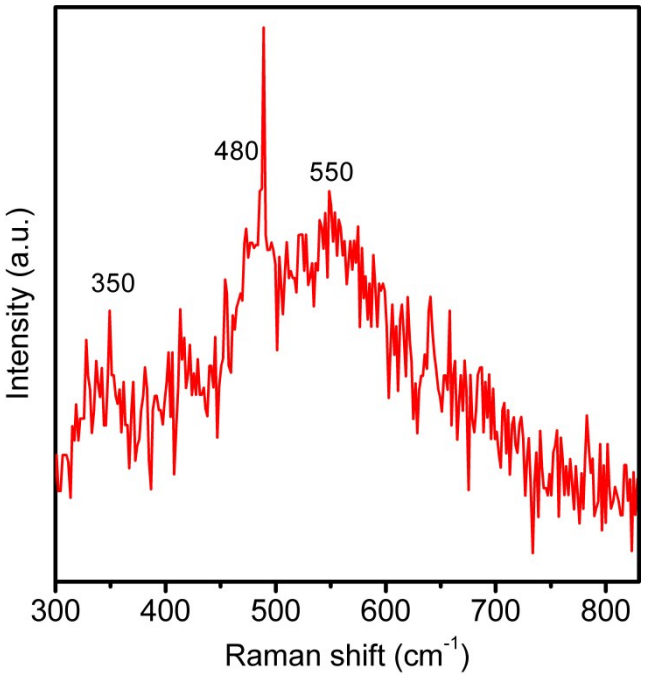

Fig. S23 Raman spectrum of Ni_3S_2/MIL-53(Fe) after OER stability test.

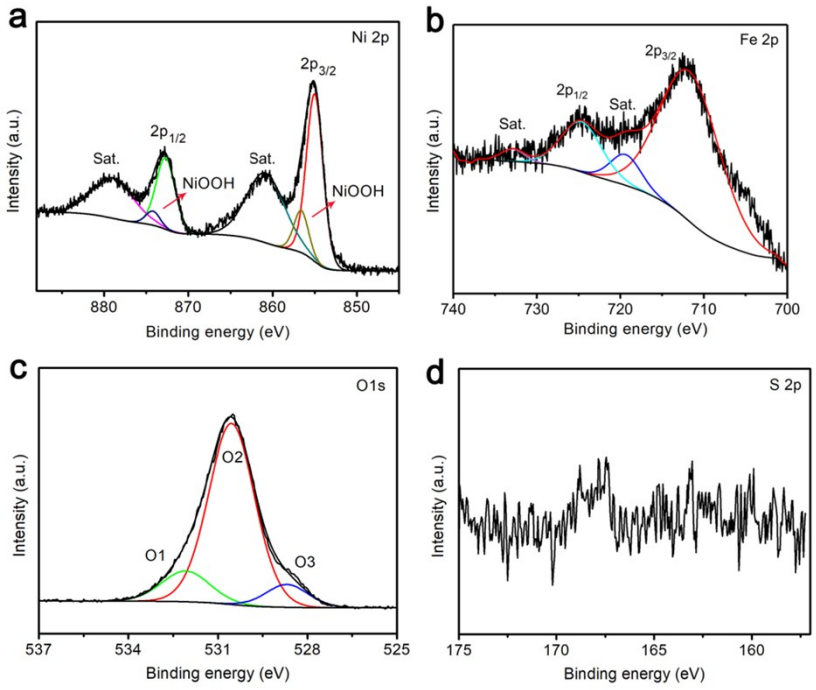

Fig. S24 High-resolution XPS spectra for the (a) Ni 2p, (b) Fe 2p, (c) O 1s, (d) S 2p of Ni_3S_2/MIL-53(Fe) after OER stability test.

Table S1. Comparison of OER performance of Ni_3S_2/MIL-53(Fe) with various sulfide-based OER electrocatalysts.

Catalyst	Electrolyte	η@10 mA cm^{-2} mV	η@100 mA cm^{-2} mV	Tafel Slope mV dec^{-1}	Stability test	Reference
Ni_3S_2/MIL-53(Fe)	1 M KOH	214	251	33.8	24 h	This work
Ni_2P-Ni_3S_2 HNAs/NF	1 M KOH	210	-	62	24 h	11
Zn-Ni_3S_2/NF	1 M KOH	-	330	87	20 h	12
CoS_2/Ni_3S_2/$CoNiO_x$	1 M KOH	256	300	43.4	one week	13
$Fe_{7.2\%}$-Ni_3S_2 NSs/NF	1 M KOH	295	-	71	10 h	14
N-$(Ni,Fe)_3S_2$/NIF	1 M KOH	167	-	33	50 h	15
S-Ni_3S_2	1 M KOH	213	286	45	60 h	16
Ni_3S_2/NF	1 M KOH	312	430	111	14 h	17
NiFe/Co_9S_8/CC	1 M KOH	219	-	55	20 h	18
Fe-Ni_3S_2/NF	1 M KOH	214	249	42	10 h	19
Ni_3S_2/Co_9S_8	1 M KOH	-	340	66	12 h	20
NiS/NiS_2	1 M KOH	-	416	156.5	24 h	21

Supplementary references

[S1] L.-L. Feng, G. Yu, Y. Wu, G.-D. Li, H. Li, Y. Sun, T. Asefa, W. Chen and X. Zou, *J. Am. Chem. Soc*., 2015, **137**, 14023-14026.

[S2] N. Jiang, Q. Tang, M. Sheng, B. You, D.-e. Jiang and Y. Sun, *Catal. Sci. Technol*., 2016, **6**, 1077-1084.

[S3] G. Zhou, H. Tian, Y. Jin, X. Tao, B. Liu, R. Zhang, Z. W. Seh, D. Zhuo, Y. Liu and J. Sun, *Proc. Natl. Acad. Sci. U. S. A.*, 2017, **114**, 840-845.

[S4] H. Shen, L. Zhang and A. Eisenberg, *J. Am. Chem. Soc.*, 1999, **121**, 2728-2740.

[S5] Y.-y. Chen, X.-j. Zhang, H.-m. Yuan, W.-t Wei and M. Yan, *Chem. Commun.*, 2013, **49**, 10974-10976.

[S6] C. Paulet, T. Loiseau, G. Férey, *J. Mater. Chem.*, 2000, **10**, 1225-1229.

[S7] M. Salavati-Niasari, H. Seyghalkar, O. Amiri, F. Davar, *J. Clust. Sci.*, 2013, **24**, 365-376.

[S8] J. Du, S. Xu, L. Sun, F. Li, *Chem. Commun.*, 2019, **55**, 14773-14776.

[S9] X. Zhao, B. Pattengale, D. Fan, Z. Zou, Y. Zhao, J. Du, J. Huang and C. Xu, *ACS Energy Lett.*, 2018, **3**, 2520-2526.

[S10] K. Rui, G. Zhao, Y. Chen, Y. Lin, Q. Zhou, J. Chen, J. Zhu, W. Sun, W. Huang and S. X. Dou, *Adv. Funct. Mater.*, 2018, **28**, 1801554.

[S11] L. Zeng, K. Sun, X. Wang, Y. Liu, Y. Pan, Z. Liu, D. Cao, Y. Song, S. Liu and C. Liu, *Nano Energy*, 2018, **51**, 26-36.

[S12] Q. Liu, L. Xie, Z. Liu, G. Du, A. M. Asiri and X. Sun, *Chem.Commun.*, 2017, **53**, 12446-12449.

[S13] H. Lee, X. Wu, Q. Ye, X. Wu, X. Wang, Y. Zhao and L. Sun, *Chem.Commun.*, 2019, **55**, 1564-1567.

[S14] Y. Zhu, H. Yang, K. Lan, K. Iqbal, Y. Liu, P. Ma, Z. Zhao, S. Luo, Y. Luo and J. Ma, *Nanoscale*, 2019, **11**, 2355-2365.

[S15] Y. Jin, X. Yue, H. Du, K. Wang, S. Huang and P. K. Shen, *J. Mater. Chem. A*, 2018, **6**, 5592-5597.

[S16] H. Zhang, H. Jiang, Y. Hu, Y. Li, Q. Xu, S. Petr and C. Li, *J. Mater. Chem. A*, 2019, **7**, 7548-7552.

[S17] G. Ren, Q. Hao, J. Mao, L. Liang, H. Liu, C. Liu and J. Zhang, *Nanoscale*, 2018, **10**, 17347-17353.

[S18] C. Zhan, Z. Liu, Y. Zhou, M. Guo, X. Zhang, J. Tu, L. Ding and Y. Cao, *Nanoscale*, 2019, **11**, 3378-3385.

[S19] G. Zhang, Y.-S. Feng, W.-T. Lu, D. He, C.-Y. Wang, Y.-K. Li, X.-Y. Wang and F.-F. Cao, *ACS Catal.*, 2018, **8**, 5431-5441.

[S20] J. Lin, H. Wang, X. Zheng, Y. Du, C. Zhao, J. Qi, J. Cao, W. Fei and J. Feng, *J. Power Sources*, 2018, **401**, 329-335.

[S21] Q. Li, D. Wang, C. Han, X. Ma, Q. Lu, Z. Xing and X. Yang, *J. Mater. Chem. A*, 2018, **6**, 8233-8237.